Heliyon 10 (2024) e31726

Contents lists available at ScienceDirect

Heliyon

journal homepage: www.cell.com/heliyon

Research article

Photoacoustic method for measuring the elasticity of polydimethylsiloxane at various mixing ratios

Tsu-Wang Shen [a,b], Ming-Chun Tsai [a], Ting-Mao Chen [a], Chi-Chang Chang [c,d,*]

[a] Department of Automatic Control Engineering, Feng Chia University, Taichung, Taiwan, ROC
[b] Master's Program Biomedical Informatics and Biomedical Engineering, Feng Chia University, Taichung, Taiwan, ROC
[c] School of Medical Informatics, Chung Shan Medical University & IT Office, Chung Shan Medical University Hospital, Taichung, Taiwan, ROC
[d] Department of Information Management, Ming Chuan University, Taoyuan, Taiwan, ROC

ARTICLE INFO

Keywords:
Photoacoustic elastography imaging
Cross-correlation method
Cardiovascular vessels
Polydimethylsiloxane (PDMS)

ABSTRACT

Measuring elasticity without physical contact is challenging, as current methods often require deconstruction of the test sample. This study addresses this challenge by proposing and testing a photoacoustic effect-based method for measuring the elasticity of polydimethylsiloxane (PDMS) at various mixing ratios, which may be applied on the wide range of applications such as biomedical and optical fields. A dual-light laser source of the photoacoustic (PA) system is designed, employing cross-correlation signal processing techniques. The platform systems and a mathematical model for performing PDMS elasticity measurements are constructed. During elasticity detection, photoacoustic signal features, influenced by hardness and shapes, are analyzed using cross-correlation calculations and phase difference detection. Results from phantom tests demonstrate the potential of predicting Young's modulus using the cross-correlation method, aligning with the American Society for Testing and Materials (ASTM) standard samples. However, accuracy may be affected by mixed materials and short tubes. Normalization or calibration of signals is suggested for aligning with Young's coefficient.

1. Introduction

Polydimethylsiloxane (PDMS), a nontoxic organosilicon component that belongs to the well-known organosilicon group, stands as a cornerstone material across a spectrum of engineering disciplines, revered for its versatility and adaptability. From mechanical and civil engineering to electronics and biomedicine [1], PDMS boasts attributes like cost-effectiveness, transparency, thermal stability, and biocompatibility, making it indispensable in a myriad of applications [2] used daily such as synthetic fibers, plastic products, lenses, glues, and micro-fluidic devices [1]. The ability to tailor its hardness by adjusting curing agent ratios further enhances its utility, rendering it invaluable in the fabrication of diverse products [3]. Despite its widespread use, real-time elasticity measurement without sample deconstruction remains a challenge. The quest for non-contact elasticity measurement methods drives the exploration of innovative techniques capable of preserving sample integrity while delivering precise measurements.

PDMS is used for phantom preparation in various imaging and elasticity studies [4,5], because it is transparent and has an approximate refractive index value of 1.43, an acoustic impedance of 150 KRayls, and a sound velocity of approximately 1300 m/s [6,

* Corresponding author. School of Medical Informatics, Chung Shan Medical University & IT Office, Chung Shan Medical University Hospital, Taichung, Taiwan, ROC.
E-mail address: changintw@gmail.com (C.-C. Chang).

https://doi.org/10.1016/j.heliyon.2024.e31726
Received 10 March 2024; Received in revised form 19 May 2024; Accepted 21 May 2024
Available online 22 May 2024

7]. Therefore, the characteristics of polydimethylsiloxane composites become important and measured by many researches [8–12] and they are often made as the phantom of blood vessels [7]. Per the laws of elasticity and biomechanics, a sample generates responses related to phenomena such as the redistribution of morphological displacements, strain, and velocity [13]. Through the use of appropriate detection methods, the strain distribution within a tissue sample can be determined to enable imaging with high imaging depth and high resolution [14,15]. Regarding mechanical properties, pure PDMS usually shows an elastic modulus between 1.32 and 2.97 MPa and tensile strength from 3.51 to 5.13 MPa [3]. However, challenges persist in achieving accurate measurements on Young's coefficient, particularly in heterogeneous materials like PDMS.

The photoacoustic (PA) effect is a process where light absorption by objects generates ultrasound waves that was discovered by Alexander Graham Bell [16] in 1880. This phenomenon involves an irradiated sample generating sound waves due to local vibration and material absorption. Because the energy of a local vibration is dependent on the level of light absorption, PA signals can provide information regarding the composition and structure of a substance. By analyzing the amplitude and phase of the resulting PA signal, light absorption and viscoelastic properties can be determined simultaneously. Lock-in amplifiers and an analog Fourier transformer were used to capture amplitude and phase differences, thereby allowing for the computation of viscoelasticity properties [17,18]. The hardware circuit can be designed to filter and capture the phase that matches the reference signal [19,20]. Chen et al. developed an algorithm that uses sound propagation model combined with time-dependent PA intensity to correct the phase deviation caused by uneven tissue surfaces [21]. The piezoelectric elements sense the ultrasound waves. While directly inserting a piezoelectric element into the human body for photoacoustic elastography might be challenging, various alternative methods exist to apply this technique for tissue diagnosis, cancer staging, and therapy. These methods involve surface measurements [22,23], external probes [24], endoscopic approaches [25,26], the integration of multiple imaging modalities [27] to assess photoacoustic images accurately, and miniature sensors (such as optical fiber) [28–30]. However, the PA signals can provide more information other than the structure of a substance.

Elastography involves deforming or displacing a tissue sample through the application of an external ultrasound force and evaluating the vibration response. Subsequently, mathematical models can be applied to solve the resulting mechanical response on the elastic modulus distribution of the organizational structure being studied [31]. Photoacoustic elastography emerges as a promising solution, leveraging the photoacoustic effect to assess elasticity. PA imaging has been instrumental in detecting tissue characteristics, such as early-stage atherosclerosis [31] and liver cirrhosis [32]. Previous studies have demonstrated the potential of PA elastography in mapping tissue elasticity noninvasively. Especially, elasticity assessments are essential for clarifying and characterizing the physiological and pathological states of tissues, and the elastic properties of tissues provide information that is essential for diagnosis,

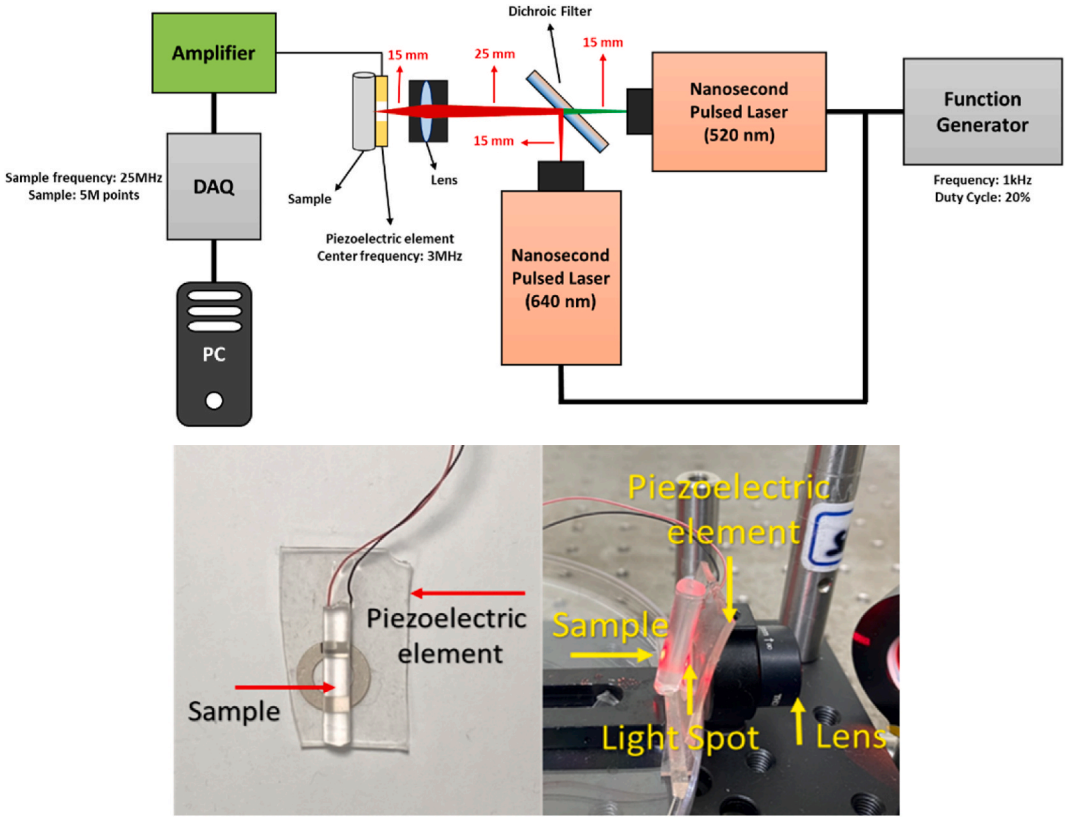

Fig. 1. PA system architecture.

cancer staging, therapy [15], and cerebrovascular assessment.

Validation studies were carried out in tissue by using shear imaging [19,20], which Young's modulus is related to the shear modulus in soft tissue. Few studies have investigated PA elastography imaging [15]. They mapped the absolute values of Young's modulus in vivo tissue up to 6-mm deep. Hai et al. [33] first demonstrated by photoacoustic elastography imaging the strains of single-layer and bilayer gelatin phantoms with various stiffness values with an average error of less than 5.2 %. Zhao et al. applied PA elastography by using a fiber-coupled continuous-wave laser (operating wavelength, 808 nm) to generate thermal stress and recording it with an ultrasound sensor [17]. Hence, how to apply the PA signals and signal processing techniques for providing more information on PA imaging such as real-time elasticity measurement becomes important issues.

The elasticity measurement may not always be feasible in a water tank environment. Thus, this study proposed a dry environment PA system which includes a dual-light source PA system to compare with a single-light source system for measuring PDMS elasticity and using signal processing techniques to enhance the elastic features in a standard desktop environment, thereby producing results that can be compared with Young's modulus from universal material testing machine.

2. Materials and methods

2.1. PA elasticity detection system

The proposed PA elasticity detection system comprises a piezoelectric sensor (STEMINC, FL, USA) coated with PDMS as PA sensor for dry PA measurement, a data acquisition card (PCIE-1840 card, Advantech, Taiwan) linked to a computer with a 25 MHz sampling rate, amplifier circuits, and pulsed lasers (NPL640 and NPL520, Thorlab, USA), which are controlled by a single signal generator to synchronize laser pulses. Fig. 1 shows a 600-nm dichroic shortpass filter (Edmund Optics, NJ, USA) that provides the transparence of a 520-nm wavelength and reflects a 640-nm wavelength laser. The filter, which had a >97 % reflection rate (average polarization), was used to mix two-wavelength laser beams that were further focused by a lens (focal length, 15 mm) to ensure that a given test sample was irradiated by the laser pulses to induce the PA effect. The ultrasonic wave generated from the analyte was transmitted to an external piezoelectric ceramic chip (center frequency, 3 MHz), where it was converted into an electrical signal (i.e., PA wave). After amplification was performed, the data acquisition card (PCIE-1840-AE, Advantech, Taiwan) digitized the signal to a computer for data analysis. The system architecture for this process is presented in Fig. 1.

2.2. Phantom preparation

2.2.1. ASTM sample preparation

ASTM International (formerly known as the American Society for Testing and Materials) publishes voluntary consensus technical standards in the form of documents covering a diverse range of materials, products, systems, and services [34]. The mechanical

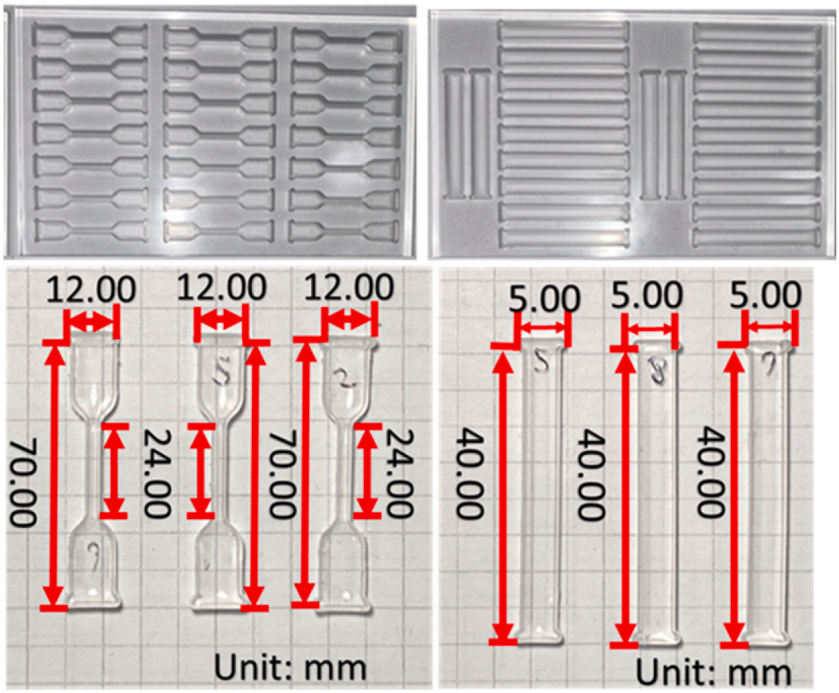

Fig. 2. ASTM D412 standard sample (Type A, left image) and cuboid sample (Type B, right image).

characterization of numerous materials is usually performed per ASTM standards.

ASTM D412, the standard test method for determining the tensile properties of vulcanized rubber and thermoplastic elastomers [35], was applied in our PDMS tension test. The thickness of the ASTM standard sample was set as 3.0 ± 0.02 mm, the test temperature was set as 23 °C ± 2 °C, and the humidity level was set as is 50 % ± 5 % RH. The distance from the narrow area of the standard sample to its center was 25 mm. A tensile test of the sample indicated a tensile speed of 500 mm/min. If the yield point elongation was <20 %, the tensile speed was set as 50 ± 5 mm/min, and if the yield point elongation was still <20 %, the tensile speed was further reduced to 5 ± 0.5 mm/min.

Our ASTM sample was prepared as follows. First, a mold was made from acrylic material by using a computer numerical control machine. To avoid dents or nicks in the sensitive neck area, which can be caused by a round cutting tool, the mold had to be rounded and over-cut at both acute and right-angled positions. The radius of the over-cut part was half the radius of the cutting tool. The ASTM D412 standard sample (Type A) and the self-made cuboid (40 × 5 × 2 mm^3; Type B) were created (Fig. 2). When the mold was filled with PDMS liquid, the Type A and Type B samples weighed approximately 0.24 ± 0.05 and 0.42 ± 0.05 g, respectively (see Fig. 3).

Type A and Type B samples were made at three elasticity levels by adjusting the PDMS-base-to-catalyst ratio (i.e., 10:5 [M1 sample], 10:2 [M2 sample], and 10:1 [M3 sample]). The mixing process took 15 min to complete, and the curing process occurred over 2 days at a temperature of 23 °C. Each type goes through the same production process with three samples for each hardness. Hence, total has 45 samples for the entire experiment. After the samples were prepared, tensile testing was conducted using microcomputer-controlled universal tensile testers (Universal Tensile Testers-CY-6102, Chun Yen Testing Machines, Taiwan) to measure Young's modulus [35–37]. Young's modulus, also known as the modulus of elasticity in tension, is a mechanical property that quantifies the tensile stiffness of a solid material. It indicates the relationship between tensile stress (force per unit area) and axial strain (proportional deformation) in the linear elastic region of a material. Notably, increasing the quantity of the catalyst used does not necessarily result in a proportional increase in hardness because of chemical characteristics. A study reported that the PDMS-base-to-catalyst ratios of 10:1, 10:2, 10:3 correspond to the Young's modulus values of 1.527, 1.334, 1.587, respectively [38]. However, Salzbrenner's research shows temperature at 70 °C for 2 h to make PDMS with 10:1 ratio with elastic modulus range from 0.39 to 0.47 MPa [39], the research provides a table to list that the PDMS-base-to-catalyst ratios of 10:1, 9:1, 8:1, 7:1, and 6:1 correspond to the Young's modulus values of 1.47, 1.53, 1.34, 1.2, and 0.93 MPa with heating process for 12 h.

2.2.2. *Stretching test*

The Type A and Type B samples were tested per ASTM D412 specifications at a tensile speed of 5 ± 0.5 mm/min on a universal material testing machine (Ju Yen CY-6102 0–2000 kg, Chun Yen Testing Machines, Taiwan). The environment temperature and humidity were maintained at 23 °C and 50 %, respectively. Each test was repeated three times to generate load/strain curves. Given that three mixture ratios were tested, a total of 18 tests were performed. All tensile tests were completed within 4 h to prevent any possible changes in sample elasticity over time. Our experiment was made when PDMS samples is placed the on the table without any tension. The results of this photoacoustic method when PDMS is under tension is not collected.

2.2.3. *Tube phantom*

Instead of evaluating pure PDMS rods, we evaluated PDMS cardiovascular vessels filled with hemoglobin chemical compound to measure Young's modulus. The mixture ratios that were applied were the identical to those applied for the Type A and Type B samples.

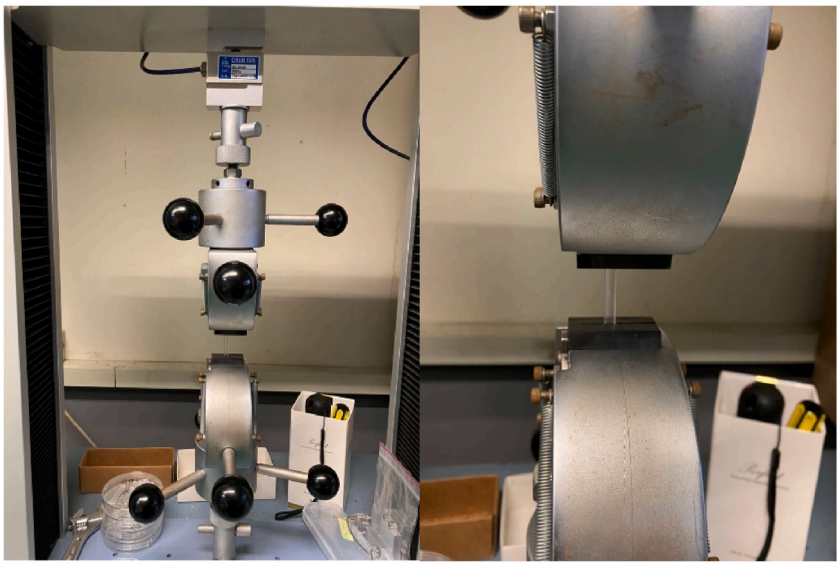

Fig. 3. Microcomputer-controlled universal tensile testers for measuring Young's modulus.

Each vessel phantom had an inner radius of 2.5 mm, outer radius of 6 mm, height of 15 mm, and weight of 0.75 ± 0.02 g (Fig. 4). Biopsy punches (World Precision Instruments-WPI, 504648) were used to punch a central hole (radius, 2.5 mm; depth, 2.5 mm) that was subsequently filled with hemoglobin solution. The solution used to fill the cardiovascular vessel phantoms was prepared by dissolving human hemoglobin (Sigma H-7379, Merck, Darmstadt, Germany) in a 0.1-M phosphate-buffered saline solution (UR-PBS001-1L, UniRegion Bio-Tech, Taiwan) at a concentration of 20 g/mL (see Fig. 5).

2.3. PA signal processing

2.3.1. PA signals

The system sampling frequency was set to 25 MHz, the number of samples was set to 5 M points, the sampling time was set to 0.2 s, the laser frequency was set to 1 kHz, and the duty cycle was set to 20 %. Two hundred waves were measured at once for each samples, with 25,000 points forming a single data piece. We obtained the eigenvalues for 200 waves of data. To minimize interference and optimize our signal assessment, a 10-level bandpass filter was designed to remove 60-Hz noise.

2.3.2. Cross-correlation

In signal processing, cross-correlation is a measure used to express the similarity between two signals, and it is usually used to identify characteristics in an unknown signal by comparing it with a known signal. It is also a function of the time between two signals (also referred to as the "sliding dot product"), being applicable in pattern recognition and cryptanalysis. For the discrete functions x and y, the cross-correlation can be expressed as formula (1). When the sequence is normalized such that the autocorrelation at zero lag equals 1, formula (2) is obtained.

$$\widehat{R}_{xy}(m) = \sum_{t=-\infty}^{\infty} f^{*}[t]g[t+m] \tag{1}$$

$$\widehat{R}_{xy,coeff}(m) = \frac{1}{\sqrt{\widehat{R}_{xx}(0)\widehat{R}_{yy}(0)}}\widehat{R}_{xy}(m) \tag{2}$$

In formulas (1) and (2), m represents the amount of translation performed. Function f[t] and $g(x)$ represent the PA signal segments. After $g(x)$ is shifted to the left m times through integration or summation, the function values of x and y after translation within the entire time domain is calculated by summing the products at any time point; e is the sum corresponding to m, and $\widehat{R}_{xy}(m)$ thus represents the correlation as distributed across different values of m.

2.3.3. Phase difference calculation

A phase difference calculation was used to calculate the delay between two signals. This calculation is performed by first removing the DC offset to prevent the frequency domain from concentrating at the zero point after Fourier transformation. Subsequently, the position of the maximum value within the frequency domain is identified, converted into radians, subtracted from the corresponding values in the two signals, and finally output into degrees.

$$X = X - X_{mean} \tag{3}$$

$$X_k = \sum_{n=0}^{N-1} X_n e^{-i2\pi k\frac{n}{N}} \tag{4}$$

$$\mathrm{Deg} = \frac{180}{\pi} \times \left(Angle_{Max_{X_{k1}}} - Angle_{Max_{X_{k2}}}\right) \tag{5}$$

where X_k is the Fourier amplitude, Deg is the angle difference between two signals, and Angle is the angle from signal k1 or k2.

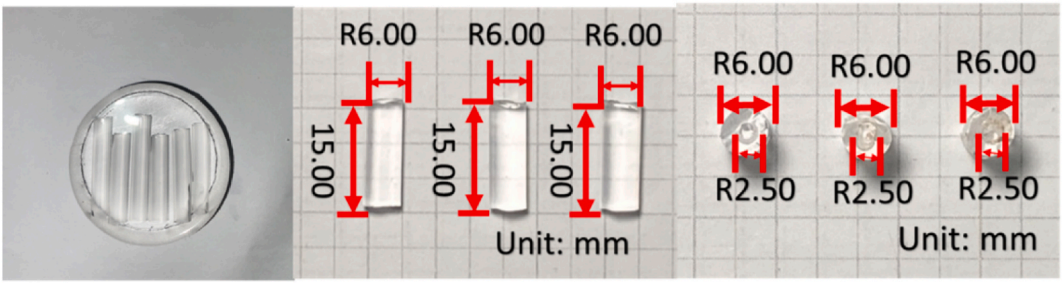

Fig. 4. A 15-mm solid round tube sample (Type C, left image) and a 15-mm hollow round tube sample (Type D, right image).

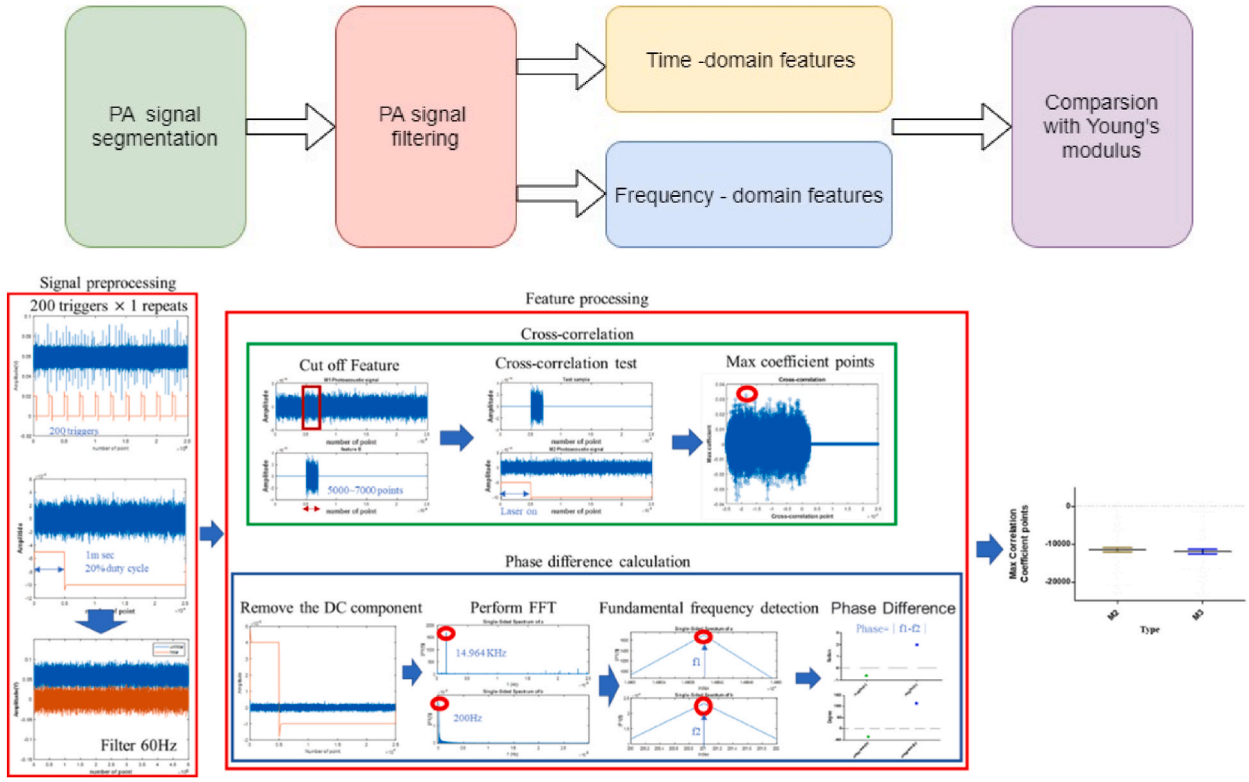

Fig. 5. System structure and signal processing steps.

2.3.4. *Comparison of the PA parameters and Young's modulus*

When biological tissue is irradiated with a laser, it absorbs light, resulting in a sinusoidal temperature change due to a non-radiative transition, which then causes thermal expansion and contraction and generates PA waves. During this process, the periodic heating of a local area causes thermal stress, and the resulting strain then generates PA waves through a force-based mechanism. Because of the damping effect of biological tissue, PA signals delay the excitation laser [14,15]. In soft tissue and human tissue, biological tissue hardness is positively correlated with shear wave propagation velocity (c), Young's modulus (E), and density (ρ), thus the formula for estimating the elasticity of a viscoelastic body can be expressed as formula (6) [40], and given that the shear wave velocity is proportional to hardness, the relationship between the phase delay δ and the viscoelastic ratio can be expressed as formula (7).

$$E = 3\rho c_s^2 \tag{6}$$

$$\delta = \arctan\frac{\eta\omega}{E} \tag{7}$$

In formula (7), η is the viscosity coefficient, which is approximately equal to 10 cst; ω is the modulation frequency; and E is Young's modulus. This formula indicates that phase delay changes in proportion to changes in Young's modulus.

2.4. *Statistical analysis*

The mean and standard deviation of the 200 feature values obtained in each detection were obtained to compare the effects of various methods. These two statistical quantities are defined as follows.

$$\overline{X} = \frac{X_1 + X_2 + \cdots + X_n}{n} \tag{8}$$

$$SD = \sqrt{\frac{1}{n}\sum_{i=1}^{N}(x_i - \overline{X})^2} \tag{9}$$

$X_1 + X_2 + \cdots + X_n$ is a set of samples, and the mean $\overline{X}$ is obtained by dividing the sum of the sample values by the number of samples.

Three sets of arrays were obtained per test. Each set contained 200 eigenvalues that were subject to one-way analysis of variance for intergroup comparisons. Therefore, post hoc tests had to be conducted, and Tukey's multiple comparison test (Tukey's honestly

significant difference) was used to test for the two data sets with the largest difference in average values within paired data sets. In this test, the q statistic was used to determine whether the difference between two groups was significant.

3. Results

Zero correction was performed prior to testing, and the spare parts were used for trial clamping to obtain two types of load/strain curves that corresponded to the three mixing ratios. Fig. 6 presents (a) two types of M1 load/strain curves, (b) the load/strain curve of the two types of M2, and (c) the load/strain curve of the two types of M3. The testing process revealed that M2 had the highest load bearing capacity and that M3 had the largest extension. Young's modulus can be calculated by applying Hooke's law. Table 1 shows the machine test results with different mixing ratios of PDMS.

3.1. Wavelength detection

Comparing with single-light-source system, dual-light-source detection systems were the most accurate in terms of cross-correlation. Through an analysis of the cross-correlation of the three ratios with the reference signal, the error value was revealed to be the smallest under the dual-light-source system. Therefore, in the present study, a dual-light-source system was used as the main detection system. To compare with single-light-source system, the dual-light-source system has two major advantages. First, two different light wavelengths expand the phase delay after cross-correlations. Second, two different light sources provide the extra light energy which can enhance the PA signals by increasing the heat expansion on samples (see Tables 2–4).

3.2. Cross-correlation

In the PA elasticity tests for the Type A, Type B, Type C, and Type D samples, cross-correlation calculations were performed for the detected signals. Cross-correlation detection proceeded in two steps. The first step was triggering a square wave to isolate section 1 (0–2500), after which the cross-correlations of the first part with various levels of hardness was calculated. The second step began with the isolation of section 2 (5000–7000) from the PA signal of M1, after which cross-correlation calculations were performed for M2 and M3. For this detection method, we considered the values from 200 wave detections and the standard deviation of 200 eigenvalues. P_{max}

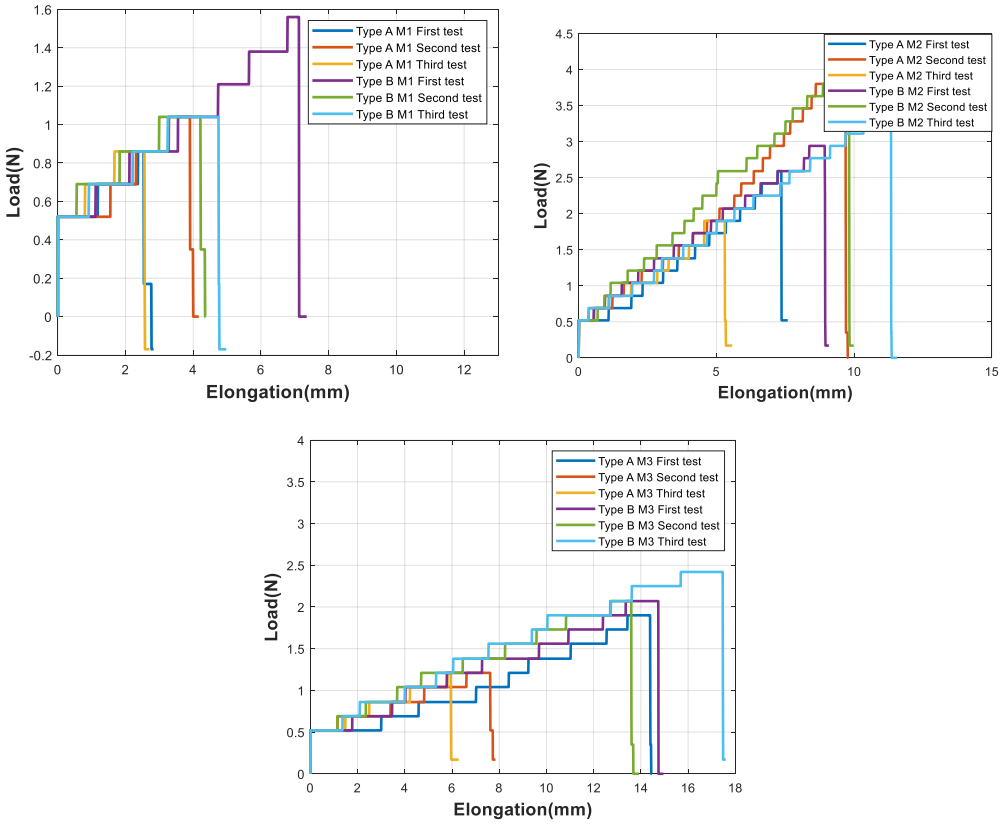

Fig. 6. Load–strain curves of the (a) Type A and (b) Type B samples.

Table 1
The Young's modulus from machine test results with different mixing ratios at curing process occurred over 2 days at a temperature of 23 °C.

Type	Mixing ratio	Young's Modules (kgf/mm^2)	Young's Modules (MPa)
Type A	M1[10:5]	0.0612 ± 0.0259	0.600 ± 0.2542
	M2[10:2]	0.0998 ± 0.0854	0.9788 ± 0.8375
	M3[10:1]	0.0372 ± 0.0155	0.3648 ± 0.1520
Type B	M1[10:5]	0.1064 ± 0.0803	1.0435 ± 0.7875
	M2[10:2]	0.1384 ± 0.638	1.3577 ± 0.1500
	M3[10:1]	0.0451 ± 0.0217	0.4421 ± 0.2127

1 kgf/mm^2 = 9.8067 MPa.

Table 2
Dual-light-source system provides smaller errors to compare with single-light-source system.

Systems	Mixing ratio	Max/Minimum Correlation coefficient	Relative position of points
Dual light sources	M1	0.2362/-0.3817	0/-6
	M2	0.2398/-0.2286	0/-15
	M3	0.3336/-0.2270	0/5
Single light source	M1	0.4182/-0.1836	−1/642
	M2	0.6504/-0.1353	0/632
	M3	0.6501/-0.2185	0/11

Table 3
Points with maximum correlation coefficient in first section.

Feature I				
Standard	Trigger of Photoacoustic Signal			
Test product				
Type	Type A	Type B	Type C	Type D
Item	mean± SD(Points)	mean± SD(Points)	mean± SD(Points)	mean± SD(Points)
M1 Feature	−4857 ± 392.4	−4238 ± 350.1	−4614 ± 451.4	−7147 ± 621.1
M2 Feature	−3880 ± 213.5	−6205 ± 516.2	−5159 ± 563.4	−4252 ± 435.3
M3 Feature	−9351 ± 689.6	−3703 ± 219.4	−6070 ± 556.3	−4222 ± 3339

Table 4
Differences between the M2 and M3 characteristics of the four sample types.

Difference between M2 and M3 characteristic	
	Feature
Type	mean ± SD(Points)
Type A	1117 ± 18.5
Type B	612 ± 14.0
Type C	576 ± 9.5
Type D	109 ± 91.9

represents the point with the maximum correlation coefficient. The following table presents the first step and lists the means and standard deviations for various levels of hardness in section 1.

The statistical distribution of the first step is presented in Fig. 7, which illustrates the 200-fold cross-correlation feature distributions for Type A, Type B, Type C, and Type D at the three ratios. These results indicate that in first section, the sample types differed in their characteristics. In Type A, M2 had the largest value, whereas in Type B, M2 had the smallest eigenvalue. That causes from value orders revised at Type A and B. In Type C and Type D, M1 had the smallest value. In addition, one-way ANOVA was performed to determine whether the sample characteristics were related at various levels of hardness. In the present study, differences between different levels of hardness were expected. In Type A and Type B, significant differences were identified between M2 and M3 and between M1 and M3. By contrast, no significant difference among M1, M2, and M3 was identified in Type C and Type D. With those significant difference results, that demonstrates the cross-correlation method based on photoacoustic signals may only show the hardness relationship within the same structure. However, the different structure samples or samples with compound solution may not

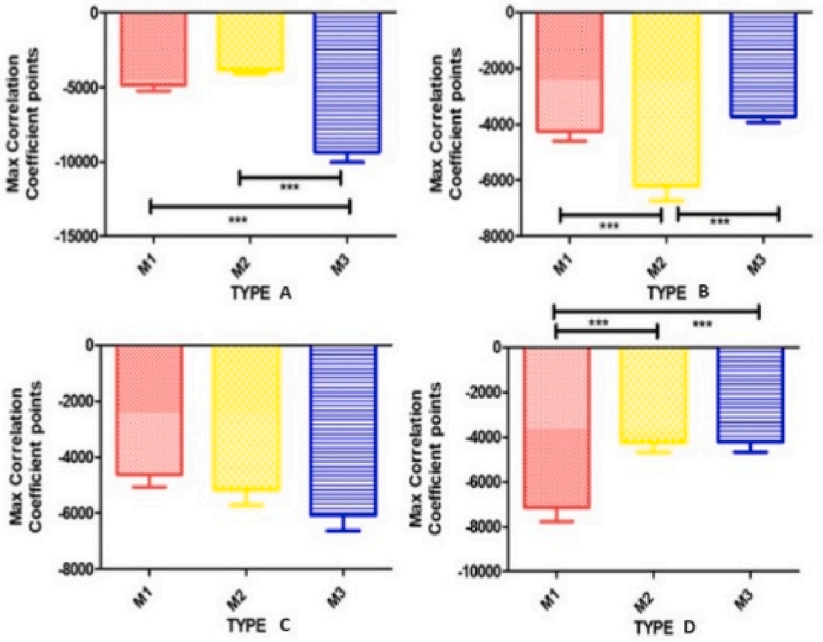

Fig. 7. Cross-correlation feature distributions of (a) Type A, (b) Type B, (c) Type C, and (d) Type D samples.

be compared to each other or provide non-significant results.

These results indicate that different types of samples with the same characteristics exhibited relative comparison of hardness.

4. Discussion

The cross-correlation and phase difference results revealed that the cross-correlation method yielded the most favorable results. The first step of cross-correlation involves using a trigger as the reference signal to identify the characteristic value distribution for minimum hardness. However, in the present study, we discovered that changes in the shape of a sample led to changes in the distribution of its characteristic values. For identical cuboid samples, no significant difference was identified. However, this was not the case for round tubes. Fig. 8 presents the distribution of the values of the four types of samples at a hardness level of M1, revealing that the Type A and Type B samples did not significantly differ from each other. In contrast, significant differences were identified between Type C and Type D samples. A value distribution similar to that of the M1 hardness can be judged by the shape and feature value. The hemograbin solution and shortened tube shape may influence the performance of the cross-correlation method, so the hardness level cannot be predicted correctly.

In accordance with the second step of the aforementioned cross-correlation method, a relationship was identified between the position of the largest cross-correlation coefficient and Young's modulus in Type A. Polynomials were generated by fitting the data to exponential functions, Gaussian functions, linear functions, and Fourier series–based functions relating the characteristics and hardness of the samples. For the Fourier series method, R2 = 1 was the optimal solution. Thus, formula (10) was obtained, in which the coefficients were $a_0 = 0.0839$, $a_1 = -0.0248$, $b_1 = -0.1202$, and $\omega = 0.005583$. With a standard product, the generated characteristic value corresponded to the standard value of the Young's modulus of the sample (see Fig. 9).

The general model $f(x)$ established using the Fourier equation was as follows,

$$f(x) = a_0 + a_1 * \cos(x * \omega) + b_1 * \sin(x * \omega) \tag{10}$$

The test results obtained through the second step of cross-correlation revealed that the standard deviation of the round tube with hemoglobin solution was smaller than that of the solid round tube. In addition, we also discovered that the PA differences in sample characteristics changed when the shape of the samples changed. When the round tube was shortened, the differences in sample characteristics between different levels of cross-correlation points decreased.

In addition, the present study also proposed a feature normalization method. Because different shape features are represented differently, errors may occur when converting these features into hardness values. Therefore, the difference between the M2 and M3 feature values of Type A was used as a reference for the new detection process. To obtain the maximum feature value (F_{max}) and minimum feature value (F_{min}) for conversion into floating values that correspond to elastic conversion, a ratio must be enlarged K times, after which the feature value is multiplied by K times to obtain the new characteristic value.

$$K = (F_{max} - F_{min}) / 505 \tag{11}$$

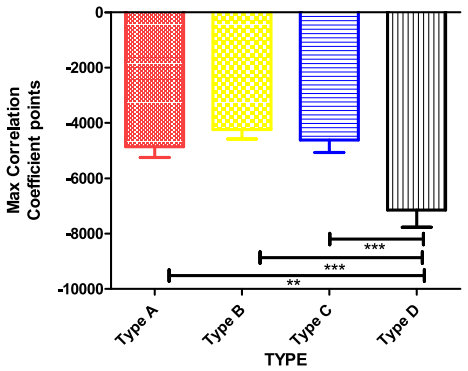

Fig. 8. Distribution of the eigenvalues of the four types of samples at the hardness level of M1.

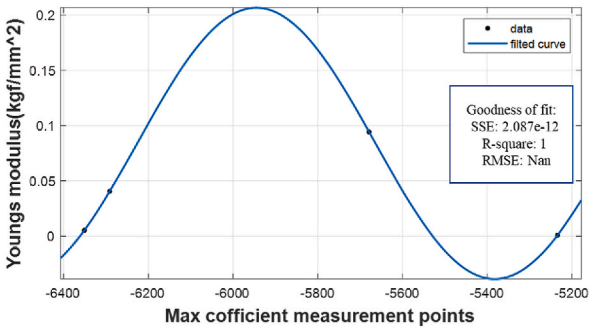

Fig. 9. The data were fit to curves to determine the relationships between the measured features and Young's modulus.

The normalization method is first used to obtain the magnification K value and calculate new characteristic values (Table 5). The table reveals that the K values of various shapes were either enlarged or reduced.

5. .Limitation

Unlike the Young's module is fixed with the material, the features from photoacustic signals may change when the shape of the sample changes, because the shape influences the ultrasound wave propagation. Different shape may cause the different propagation distances, which will influence cross-correlation results. However, PA signal indicates the hardness if the shape is determined. For data normalization according to the shape, it is suggested to use microcomputer-controlled universal tensile testers for measuring Young's modulus of one standard sample to get the initial point on formula. Then other samples with different hardness can be predicted their Young's modules by using non-contact PA signal technique.

The presence of the hemoglobin solution in Types C and D samples significantly impacts the accuracy of the Young's modulus prediction, especially for shortened round tubes. Due to shortened round tubes have the shortest ultrasound wave propagation distance, the cross-correlation method have large error on delay results, especially on M2 sample (type C). It is well-known that hemoglobin will affect light absorption around 645 nm wavelength, so it is found that the hemoglobin do have the influence on the PA signal feature. Hence, the mixed material type D also have large error on propagation delay. Unlike the Young's module tester is not affected by light, the PA non-contact measurement have its limitation on mixed materials and is required for calibration of the propagation delay based on shapes.

6. Conclusions

A dual-light source platform system and mathematical model for PDMS elasticity measurement were constructed, which can detect

Table 5
Original feature data and Young's modulus after conversion.

Type	Type C	Type D
Item	mean ± SD (Points)	mean ± SD (Points)
M2 Feature	−1478	−7138
M3 Feature	−1502	−7795

the phase delay caused by photoacoustic signal, and the phase delay varies according to hardness only if the same shape. Cross-correlation calculations and phase difference detection were used to calculate this phase delay and have been shown to provide accurate hardness detection at the same shape. Significant results are shown for the standard ASTM samples. The formula states that signal delay are correlated with hardness relationship. The PA signal of the system was generated by setting the parameters of the laser emission system and the appropriate signal filters.

The dual-light-source system was revealed to outperform the single-light-source system as a verification system with cross-correlation method. These methods yielded the position and phase difference of the maximum cross-correlation coefficient and verified the feasibility of delay through statistical analysis and feature selection.

In addition, a detection method was developed through the application of appropriate features, and the value range for PA feature was first assessed on the basis of shape. The calculation of differences and conversion at the same shape to Young's modulus were then performed, leading to an improvement in the stability of signal detection. However, the exact mechanism for PA signal changes according to shape and mixed materials is unknown. The future studies is suggested to have detail evaluation on ultrasound wave propagation on different conditions.

Funding

This research was funded by the FCU/TVGH project (grant number: TCVGH-FCU1088205) and the FCU/CSMU project (grant number: FCU/CSMU 107-001).

Data availability statement

The data will be made available upon request.

CRediT authorship contribution statement

Tsu-Wang Shen: Writing – review & editing, Writing – original draft, Supervision, Conceptualization. **Ming-Chun Tsai:** Visualization, Methodology, Investigation, Formal analysis. **Ting-Mao Chen:** Visualization, Software, Methodology, Formal analysis. **Chi-Chang Chang:** Writing – review & editing, Writing – original draft, Investigation, Conceptualization.

Declaration of competing interest

The authors declare no conflict of interest.

References

[1] V.C. Pinto, G. Minas, M. Correia-Neves, PDMS biofunctionalization study for the development of a microfluidic device: application to salivary cortisol, IEEE 4th Portuguese Meeting on Bioengineering (ENBENG) (2015) 1–5, 2015.
[2] F. Sales, A. Souza, R. Ariati, V. Noronha, E. Giovanetti, R. Lima, J. Ribeiro, Composite material of PDMS with Interchangeable transmittance: study of optical, mechanical properties and Wettability, J. Compos. Sci. 5 (4) (2021) 110.
[3] R. Ariati, F. Sales, A. Souza, R.A. Lima, J. Ribeiro, Polydimethylsiloxane composites characterization and its applications: a review, Polymers 13 (23) (2021).
[4] C. Avigo, N. Di Lascio, P. Armanetti, C. Kusmic, L. Cavigli, F. Ratto, S. Meucci, C. Masciullo, M. Cecchini, R. Pini, F. Faita, L. Menichetti, Organosilicon phantom for photoacoustic imaging, J. Biomed. Opt. 20 (4) (2015) 46008.
[5] F. Ratto, L. Cavigli, C. Borri, S. Centi, G. Magni, M. Mazzoni, R. Pini, Hybrid organosilicon/polyol phantom for photoacoustic imaging, Biomed. Opt Express 10 (8) (2019) 3719–3730.
[6] M. Liu, J. Sun, Y. Sun, C. Bock, Q. Chen, Thickness-dependent mechanical properties of polydimethylsiloxane membranes, J. Micromech. Microeng. 19 (3) (2009) 035028.
[7] J.H. Kim, P. Chhai, K. Rhee, Development and characterization of viscoelastic polydimethylsiloxane phantoms for simulating arterial wall motion, Med. Eng. Phys. 91 (2021) 12–18.
[8] D.G. Auliya, U. Fauziah, V.F. Arini, S. Setiadji, F. Fitrilawati, A.S. Kartasasmita, R. Risdiana, Use of Dichlorodimethylsilane to Produce polydimethylsiloxane as a substitute for vitreous humour: characteristics and in vitro toxicity, J. Funct. Biomater. 14 (8) (2023).
[9] E. Chmielnicka, M. Szymiczek, S. Sarraj, S. Jurczyk, Analysis of thermal aging influence on selected physical and mechanical characteristics of polyaddition and polycondensation poly(dimethylsiloxane), Polymers 15 (19) (2023).
[10] N.A. Lacher, N.F. de Rooij, E. Verpoorte, S.M. Lunte, Comparison of the performance characteristics of poly(dimethylsiloxane) and Pyrex microchip electrophoresis devices for peptide separations, J. Chromatogr. A 1004 (1–2) (2003) 225–235.
[11] S.J. Lee, Y.C. Sohn, C.L. Kim, Friction and wear characteristics of polydimethylsiloxane under water-based lubrication conditions, Materials 15 (9) (2022).
[12] T.Y. Liao, P.C. King, D. Zhu, R.J. Crawford, E.P. Ivanova, H. Thissen, P. Kingshott, Surface characteristics and bone biocompatibility of cold-sprayed porous titanium on polydimethylsiloxane substrates, ACS Biomater. Sci. Eng. 9 (3) (2023) 1402–1421.
[13] J. Ophir, S.K. Alam, B. Garra, F. Kallel, E. Konofagou, T. Krouskop, T. Varghese, Elastography: ultrasonic estimation and imaging of the elastic properties of tissues, Proc. Inst. Mech. Eng. H 213 (3) (1999) 203–233.
[14] C. Li, G. Guan, X. Cheng, Z. Huang, R.K. Wang, Quantitative elastography provided by surface acoustic waves measured by phase-sensitive optical coherence tomography, Opt. Lett. 37 (4) (2012) 722–724.
[15] M.S. Singh, A. Thomas, Photoacoustic elastography imaging: a review, J. Biomed. Opt. 24 (4) (2019) 1–15.
[16] Z. Chen, S. Yang, D. Xing, In vivo detection of hemoglobin oxygen saturation and carboxyhemoglobin saturation with multiwavelength photoacoustic microscopy, Opt. Lett. 37 (16) (2012) 3414–3416.
[17] Y. Zhao, S. Yang, C. Chen, D. Xing, Simultaneous optical absorption and viscoelasticity imaging based on photoacoustic lock-in measurement, Opt. Lett. 39 (9) (2014) 2565–2568.
[18] F. Yang, S. Yang, Simultaneous photoacoustic elasticity and viscosity imaging. 2016 Asia Communications and Photonics Conference (ACP), 2016, pp. 1–3.
[19] Q. Wang, Y. Shi, F. Yang, S. Yang, Quantitative photoacoustic elasticity and viscosity imaging for cirrhosis detection, Appl. Phys. Lett. 112 (21) (2018) 211902.

[20] P. Wang, Z. Chen, F. Yang, S. Yang, D. Xing, Intravascular tri-modality system: combined ultrasound, photoacoustic, and elasticity imaging, Appl. Phys. Lett. 113 (25) (2018) 253701.
[21] C. Chen, Y. Zhao, S. Yang, D. Xing, Integrated mechanical and structural features for photoacoustic characterization of atherosclerosis using a quasi-continuous laser, Opt Express 23 (13) (2015) 17309–17315.
[22] F. Peia, N.C. Veiga, A.P. Gomes, B.N.D. Santos, N.M.S. Marques, I. Gloria, J.B. Goulardins, Effects of hippotherapy on postural control in children with cerebral palsy: a systematic review, Pediatr. Phys. Ther. 35 (2) (2023) 202–210.
[23] O. Nykänen, A. Pulkkinen, T. Tarvainen, Quantitative photoacoustic tomography augmented with surface light measurements, Biomed. Opt Express 8 (10) (2017) 4380–4395.
[24] M. Benyamin, Z. Zalevsky, All optical speckle contrast-based vibration sensor for photoacoustic signal detection, Sensors 22 (2022) 3250.
[25] B. Lengenfelder, F. Mehari, M. Hohmann, C. Lohr, M.J. Waldner, M. Schmidt, Z. Zalevsky, F. Klampfl, Contact-free endoscopic photoacoustic sensing using speckle analysis, J. Biophotonics. 12 (12) (2019) e201900130.
[26] W. Pang, Y. Wang, L. Guo, B. Wang, P. Lai, J. Xiao, Two-dimensional photoacoustic/ultrasonic endoscopic imaging based on a line-focused transducer, Front. Bioeng. Biotechnol. 9 (2021) 807633.
[27] X. Zhu, Z. Huang, Z. Li, W. Li, X. Liu, Z. Chen, J. Tian, C. Li, Resolution-matched reflection mode photoacoustic microscopy and optical coherence tomography dual modality system, Photoacoustics 19 (2020) 100188.
[28] Y. Ren, Y. Zhang, H. He, L. Liu, X. Wu, L. Song, C. Liu, Optical fiber-based handheld polarized photoacoustic computed tomography for detecting anisotropy of tissues, Quant Imaging Med Surg 12 (4) (2022) 2238–2246.
[29] D. Martin-Sanchez, J. Li, D.M. Marques, E.Z. Zhang, P.R.T. Munro, P.C. Beard, J.A. Guggenheim, ABCD transfer matrix model of Gaussian beam propagation in Fabry-Perot etalons, Opt Express 30 (26) (2022) 46404–46417.
[30] X. Zhu, Z. Huang, Z. Li, W. Li, X. Liu, Z. Chen, J. Tian, C. Li, Resolution-matched reflection mode photoacoustic microscopy and optical coherence tomography dual modality system, Photoacoustics 19 (2020) 100188.
[31] R.M.S. Sigrist, J. Liau, A.E. Kaffas, M.C. Chammas, J.K. Willmann, Ultrasound elastography: review of techniques and clinical applications, Theranostics 7 (5) (2017) 1303–1329.
[32] X. Zhang, C. Weng, S. Wu, J. Cai, H. Wu, Z. Li, L. Zhu, H. Li, Photoacoustic identification of blood vessel deformation under pressure, AIP Adv. 9 (7) (2019) 075019.
[33] Q. Wang, Y. Shi, F. Yang, S. Yang, Quantitative photoacoustic elasticity and viscosity imaging for cirrhosis detection, Appl. Phys. Lett. 112 (21) (2018) 211902.
[34] A. International, What Is ASTM International? The History of ASTM International., 2021.
[35] A.S. Cruz-Felix, A. Santiago-Alvarado, J. Marquez-Garcia, J. Gonzalez-Garcia, PDMS samples characterization with variations of synthesis parameters for tunable optics applications, Heliyon 5 (12) (2019) e03064.
[36] K. Khanafer, A. Duprey, M. Schlicht, R. Berguer, Effects of strain rate, mixing ratio, and stress-strain definition on the mechanical behavior of the polydimethylsiloxane (PDMS) material as related to its biological applications, Biomed. Microdevices 11 (2) (2009) 503–508.
[37] I.D. Johnston, D.K. McCluskey, C.K.L. Tan, M.C. Tracey, Mechanical characterization of bulk Sylgard 184 for microfluidics and microengineering, J. Micromech. Microeng. 24 (3) (2014) 035017.
[38] F.C.P. Sales, R.M. Ariati, V.T. Noronha, J.E. Ribeiro, Mechanical characterization of PDMS with different mixing ratios, Procedia Struct. Integr. 37 (2022) 383–388.
[39] J. Salzbrenner, Mechanical and Electrical Properties of Carbon Nanotubes Surface-Stamped on Polydimethylsiloxane for Microvalve Actuation, University of New Mexico, UNM's Digital Repository, 2012.
[40] M. Yamasaki, Y. Sasaki, Y. Iijima, Determining Young's modulus of timber on the basis of a strength database and stress wave propagation velocity II: effect of the reference distribution database on the determination, J. Wood Sci. 56 (5) (2010) 380–386.